NEURAL INFORMATION PROCESSING SYSTEMS

Learning High-Precision Bounding Box for Rotated Object Detection via Kullback-Leibler Divergence

Xue Yang - Shanghai Jiao Tong University

Virtual. 2021

NEURAL INFORMATION PROCESSING SYSTEMS

Two design paradigms for rotated detectors

- ➢ Induction paradigm
- ➢ Deduction paradigm

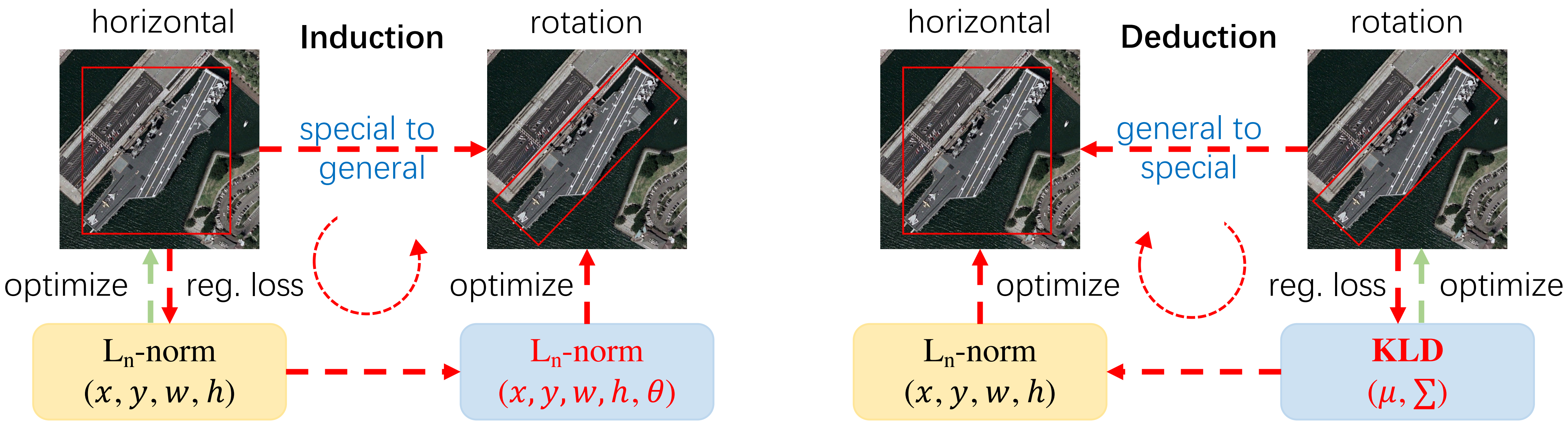

Induction paradigm

1. For horizontal bounding box regression, the model mainly outputs four items for location and size: $t_x^p = \frac{x_p - x_a}{w_a}, t_y^p = \frac{y_p - y_a}{h_a}, t_w^p = \ln\left(\frac{w_p}{w_a}\right), t_h^p = \ln\left(\frac{h_p}{h_a}\right)$ to match the four targets from the ground truth $t_x^t = \frac{x_t - x_a}{w_a}, t_y^t = \frac{y_t - y_a}{h_a}, t_w^t = \ln\left(\frac{w_t}{w_a}\right), t_h^t = \ln\left(\frac{h_t}{h_a}\right)$

2. Extending the above horizontal case, existing rotation detection models also use regression loss which simply involves an extra angle parameter

$$t_\theta^p = f(\theta_p - \theta_a), t_\theta^t = f(\theta_t - \theta_a)$$

3. The overall regression loss for rotation detection is:

$$L_{reg} = l_n\text{-norm}\left(\Delta t_x, \Delta t_y, \Delta t_w, \Delta t_h, \Delta t_\theta\right)$$

where $\Delta t_x = t_x^p - t_x^t = \frac{\Delta x}{w_a}, \Delta t_y = t_y^p - t_y^t = \frac{\Delta y}{h_a}, \Delta t_w = t_w^p - t_w^t = \ln(w_p/w_t), \Delta t_h = t_h^p - t_h^t = \ln(h_p/h_t)$, and $\Delta t_\theta = t_\theta^p - t_\theta^t = \Delta\theta$.

Deduction paradigm

$$
\begin{aligned}
\mathbf{\Sigma}^{1/2} =& \mathbf{R}\mathbf{S}\mathbf{R}^\top \\
=& \begin{pmatrix} \cos\theta & -\sin\theta \\ \sin\theta & \cos\theta \end{pmatrix} \begin{pmatrix} \frac{w}{2} & 0 \\ 0 & \frac{h}{2} \end{pmatrix} \begin{pmatrix} \cos\theta & \sin\theta \\ -\sin\theta & \cos\theta \end{pmatrix} \\
=& \begin{pmatrix} \frac{w}{2}\cos^2\theta + \frac{h}{2}\sin^2\theta & \frac{w-h}{2}\cos\theta\sin\theta \\ \frac{w-h}{2}\cos\theta\sin\theta & \frac{w}{2}\sin^2\theta + \frac{h}{2}\cos^2\theta \end{pmatrix} \\
\mathbf{m} =& (x, y)^\top
\end{aligned}
$$

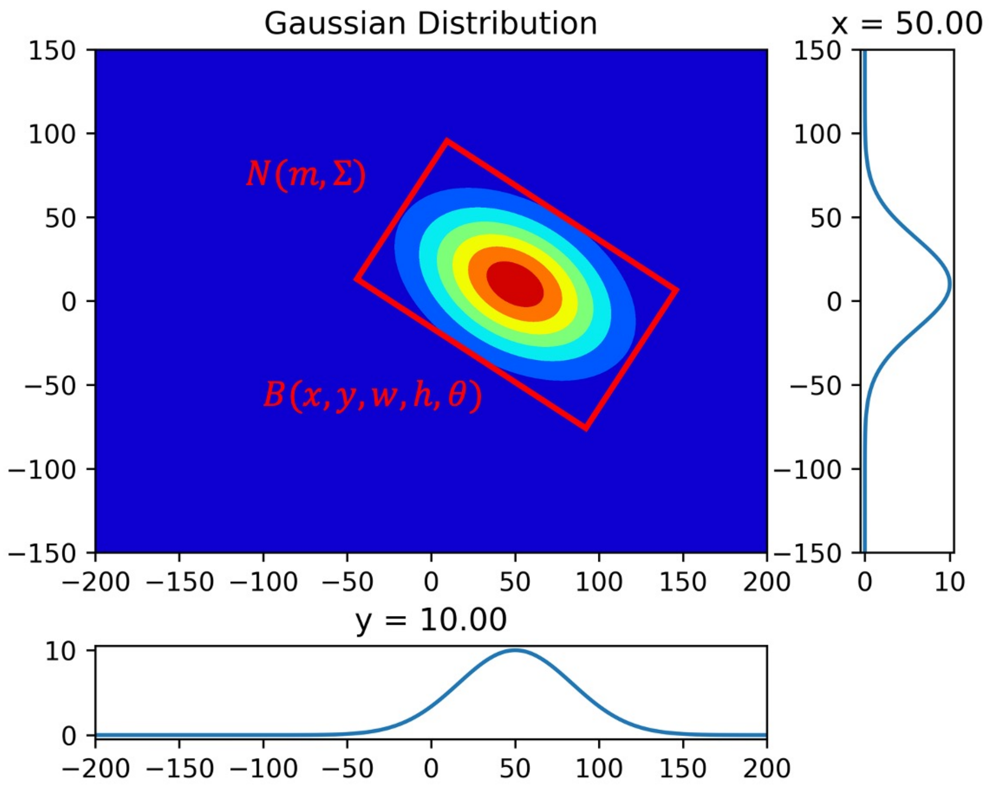

Property 1: $\mathbf{\Sigma}^{1/2}(w, h, \theta) = \mathbf{\Sigma}^{1/2}(h, w, \theta - \frac{\pi}{2})$;

Property 2: $\mathbf{\Sigma}^{1/2}(w, h, \theta) = \mathbf{\Sigma}^{1/2}(w, h, \theta - \pi)$;

Property 3: $\mathbf{\Sigma}^{1/2}(w, h, \theta) \approx \mathbf{\Sigma}^{1/2}(w, h, \theta - \frac{\pi}{2})$, if $w \approx h$.

X. Yang, et al. "Rethinking Rotated Object Detection with Gaussian Wasserstein Distance Loss." In ICML 2021.

Wasserstein Distance

- General formula :

$$\mathbf{D}_w(\mathcal{N}_p,\mathcal{N}_t)^2 = \underbrace{\|\boldsymbol{\mu}_p - \boldsymbol{\mu}_t\|_2^2}_{\text{center distance}} + \underbrace{\mathbf{Tr}(\boldsymbol{\Sigma}_p + \boldsymbol{\Sigma}_t - 2(\boldsymbol{\Sigma}_p^{1/2}\boldsymbol{\Sigma}_t\boldsymbol{\Sigma}_p^{1/2})^{1/2})}_{\text{coupling terms about } h_p,\ w_p \text{ and } \theta_p}$$

- Horizontal special case:

$$\begin{aligned}\mathbf{D}_w^h(\mathcal{N}_p,\mathcal{N}_t)^2 &= \|\boldsymbol{\mu}_p - \boldsymbol{\mu}_t\|_2^2 + \|\boldsymbol{\Sigma}_p^{1/2} - \boldsymbol{\Sigma}_t^{1/2}\|_F^2 \\ &= (x_p - x_t)^2 + (y_p - y_t)^2 + \left((w_p - w_t)^2 + (h_p - h_t)^2\right)/4 \\ &= l_2\text{-norm}(\Delta x, \Delta y, \Delta w/2, \Delta h/2)\end{aligned}$$

Kullback-Leibler Divergence

- General formula :

$$\mathbf{D}_{kl}(\mathcal{N}_p||\mathcal{N}_t) = \underbrace{\frac{1}{2}(\boldsymbol{\mu}_p - \boldsymbol{\mu}_t)^\top \boldsymbol{\Sigma}_t^{-1}(\boldsymbol{\mu}_p - \boldsymbol{\mu}_t)}_{\text{term about } x_p \text{ and } y_p} + \underbrace{\frac{1}{2}\mathbf{Tr}(\boldsymbol{\Sigma}_t^{-1}\boldsymbol{\Sigma}_p) + \frac{1}{2}\ln\frac{|\boldsymbol{\Sigma}_t|}{|\boldsymbol{\Sigma}_p|}}_{\text{coupling terms about } h_p,\ w_p \text{ and } \theta_p} - 1$$

or

$$\mathbf{D}_{kl}(\mathcal{N}_t||\mathcal{N}_p) = \underbrace{\frac{1}{2}(\boldsymbol{\mu}_p - \boldsymbol{\mu}_t)^\top \boldsymbol{\Sigma}_p^{-1}(\boldsymbol{\mu}_p - \boldsymbol{\mu}_t) + \frac{1}{2}\mathbf{Tr}(\boldsymbol{\Sigma}_p^{-1}\boldsymbol{\Sigma}_t) + \frac{1}{2}\ln\frac{|\boldsymbol{\Sigma}_p|}{|\boldsymbol{\Sigma}_t|}}_{\text{chain coupling of all parameters}} - 1$$

- Horizontal special case :

$$\begin{aligned}\mathbf{D}_{kl}^h(\mathcal{N}_p||\mathcal{N}_t) &= \frac{1}{2}\left(\frac{w_p^2}{w_t^2} + \frac{h_p^2}{h_t^2} + \frac{4\Delta^2 x}{w_t^2} + \frac{4\Delta^2 y}{h_t^2} + \ln\frac{w_t^2}{w_p^2} + \ln\frac{h_t^2}{h_p^2} - 2\right) \\ &= 2l_2\text{-norm}(\Delta t_x, \Delta t_y) + l_1\text{-norm}(\ln\Delta t_w, \ln\Delta t_h) + \frac{1}{2}l_2\text{-norm}\left(\frac{1}{\Delta t_w}, \frac{1}{\Delta t_h}\right) - 1\end{aligned}$$

High-Precision Detection （KLD>GWD>smooth L1）

1. Specific expressions of KLD's main three terms:

$$(\boldsymbol{\mu}_p - \boldsymbol{\mu}_t)^\top \boldsymbol{\Sigma}_t^{-1} (\boldsymbol{\mu}_p - \boldsymbol{\mu}_t) = \frac{4(\Delta x \cos\theta_t + \Delta y \sin\theta_t)^2}{w_t^2} + \frac{4(\Delta y \cos\theta_t - \Delta x \sin\theta_t)^2}{h_t^2}$$

$$\mathbf{Tr}(\boldsymbol{\Sigma}_t^{-1} \boldsymbol{\Sigma}_p) = \frac{h_p^2}{w_t^2} \sin^2 \Delta\theta + \frac{w_p^2}{h_t^2} \sin^2 \Delta\theta + \frac{h_p^2}{h_t^2} \cos^2 \Delta\theta + \frac{w_p^2}{w_t^2} \cos^2 \Delta\theta$$

$$\ln \frac{|\boldsymbol{\Sigma}_t|}{|\boldsymbol{\Sigma}_p|} = \ln \frac{h_t^2}{h_p^2} + \ln \frac{w_t^2}{w_p^2}$$

where $\Delta x = x_p - x_t, \Delta y = y_p - y_t, \Delta\theta = \theta_p - \theta_t$

High-Precision Detection （KLD>GWD>smooth L1）

2. Without loss of generality, we set $\theta_t = 0$， then:

$$\frac{\partial f_{kl}(\mu_p)}{\partial \mu_p} = \left(\frac{4}{w_t^2}\Delta x, \frac{4}{h_t^2}\Delta y\right)^\top$$

When $\theta_t \neq 0$, the gradient of the object offset ($\Delta \mathbf{x}$ and $\Delta \mathbf{y}$) will be dynamically adjusted according to the θ_t for better optimization. In contrast, the gradient of the center point in GWD and L2-norm are:

$$\frac{\partial f_w(\mu_p)}{\partial \mu_p} = (2\Delta x, 2\Delta y)^\top \qquad \frac{\partial f_{L_2}(\mu_p)}{\partial \mu_p} = (\frac{2}{w_a^2}\Delta x, \frac{2}{h_a^2}\Delta y)^\top$$

High-Precision Detection （KLD>GWD>smooth L1）

3. For h_p and w_p, we have

$$\frac{\partial f_{kl}(\mathbf{\Sigma}_p)}{\partial \ln h_p} = \frac{h_p^2}{h_t^2}\cos^2\Delta\theta + \frac{h_p^2}{w_t^2}\sin^2\Delta\theta - 1, \quad \frac{\partial f_{kl}(\mathbf{\Sigma}_p)}{\partial \ln w_p} = \frac{w_p^2}{w_t^2}\cos^2\Delta\theta + \frac{w_p^2}{h_t^2}\sin^2\Delta\theta - 1$$

On the one hand, the optimization of the h_p and w_p is affected by the $\Delta\theta$. When $\Delta\theta = 0$:

$$\frac{\partial f_{kl}(\mathbf{\Sigma}_p)}{\partial \ln h_p} = \frac{h_p^2}{h_t^2} - 1, \frac{\partial f_{kl}(\mathbf{\Sigma}_p)}{\partial \ln w_p} = \frac{w_p^2}{w_t^2} - 1$$

which means that the smaller targeted height or width leads to heavier penalty on its matching loss. This is desirable, as smaller height or width needs higher matching precision.

High-Precision Detection （KLD>GWD>smooth L1）

4. For θ:

$$\frac{\partial f_{kl}(\boldsymbol{\Sigma}_p)}{\partial \theta_p} = \left(\frac{h_p^2 - w_p^2}{w_t^2} + \frac{w_p^2 - h_p^2}{h_t^2} \right) \sin 2\Delta\theta$$

On the other hand, the optimization of $\Delta\theta$ is also affected by h_p and w_p. When $h_p = h_t$, $w_p = w_t$:

$$\frac{\partial f_{kl}(\boldsymbol{\Sigma}_p)}{\partial \theta_p} = \left(\frac{h_t^2}{w_t^2} + \frac{w_t^2}{h_t^2} - 2 \right) \sin 2\Delta\theta \geq \sin 2\Delta\theta$$

This shows that the larger the aspect ratio of the object, the model will pay more attention to the optimization of the angle. This is the main reason why the KLD-based model has a huge advantage in high-precision detection as a slight angle error would cause a serious accuracy drop for large aspect ratios objects.

NEURAL INFORMATION PROCESSING SYSTEMS

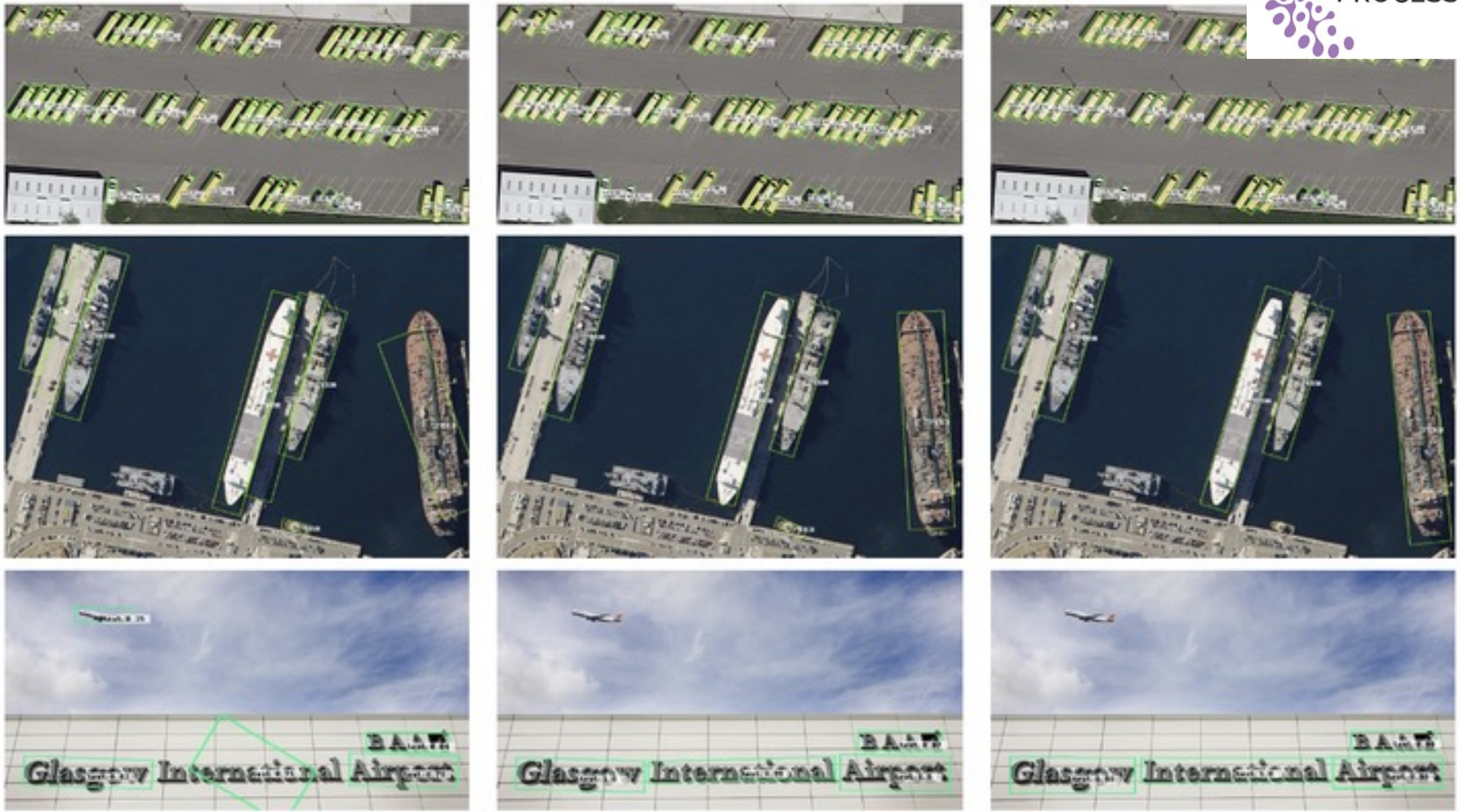

L_2 loss GWD KLD

Scale Invariance Comparison

- Obviously GWD and L_2-norm are not scale-invariant .
- For two known Gaussian distributions $\mathbf{X}_p \sim \mathcal{N}_p(\boldsymbol{\mu}_p, \boldsymbol{\Sigma}_p)$ $\mathbf{X}_t \sim \mathcal{N}_t(\boldsymbol{\mu}_t, \boldsymbol{\Sigma}_t)$ and a full-rank matrix $\mathbf{M}$ $(|\mathbf{M}| \neq \mathbf{0})$, we have：

$$\mathbf{X}_{p'} = \mathbf{M}\mathbf{X}_p \sim \mathcal{N}_p(\mathbf{M}\boldsymbol{\mu}_p, \mathbf{M}\boldsymbol{\Sigma}_p\mathbf{M}^\top), \mathbf{X}_{t'} = \mathbf{M}\mathbf{X}_t \sim \mathcal{N}_t(\mathbf{M}\boldsymbol{\mu}_t, \mathbf{M}\boldsymbol{\Sigma}_t\mathbf{M}^\top)$$

- We mark them as $\mathcal{N}_{p'}$ and $\mathcal{N}_{t'}$, then their KLD is calculated as follows:

$$\begin{aligned}
\mathbf{D}_{kl}(\mathcal{N}_{p'}||\mathcal{N}_{t'}) &= \frac{1}{2}(\boldsymbol{\mu}_p - \boldsymbol{\mu}_t)^\top \mathbf{M}^\top(\mathbf{M}^\top)^{-1}\boldsymbol{\Sigma}_t^{-1}\mathbf{M}^{-1}\mathbf{M}(\boldsymbol{\mu}_p - \boldsymbol{\mu}_t) \\
&+ \frac{1}{2}\mathbf{Tr}\left((\mathbf{M}^\top)^{-1}\boldsymbol{\Sigma}_t^{-1}\mathbf{M}^{-1}\mathbf{M}\boldsymbol{\Sigma}_p\mathbf{M}^\top\right) + \frac{1}{2}\ln\frac{|\mathbf{M}||\boldsymbol{\Sigma}_t||\mathbf{M}^\top|}{|\mathbf{M}||\boldsymbol{\Sigma}_p||\mathbf{M}^\top|} - 1 \\
&= \frac{1}{2}(\boldsymbol{\mu}_p - \boldsymbol{\mu}_t)^\top \boldsymbol{\Sigma}_t^{-1}(\boldsymbol{\mu}_p - \boldsymbol{\mu}_t) + \frac{1}{2}\mathbf{Tr}\left(\mathbf{M}^\top(\mathbf{M}^\top)^{-1}\boldsymbol{\Sigma}_t^{-1}\mathbf{M}^{-1}\mathbf{M}\boldsymbol{\Sigma}_p\right) + \frac{1}{2}\ln\frac{|\boldsymbol{\Sigma}_t|}{|\boldsymbol{\Sigma}_p|} - 1 \\
&= \mathbf{D}_{kl}(\mathcal{N}_p||\mathcal{N}_t)
\end{aligned}$$

- Therefore, KLD is actually affine invariance. When$\mathbf{M} = \mathbf{kI}$, the scale invariance of KLD has been proved.

Scale Invariance Comparison

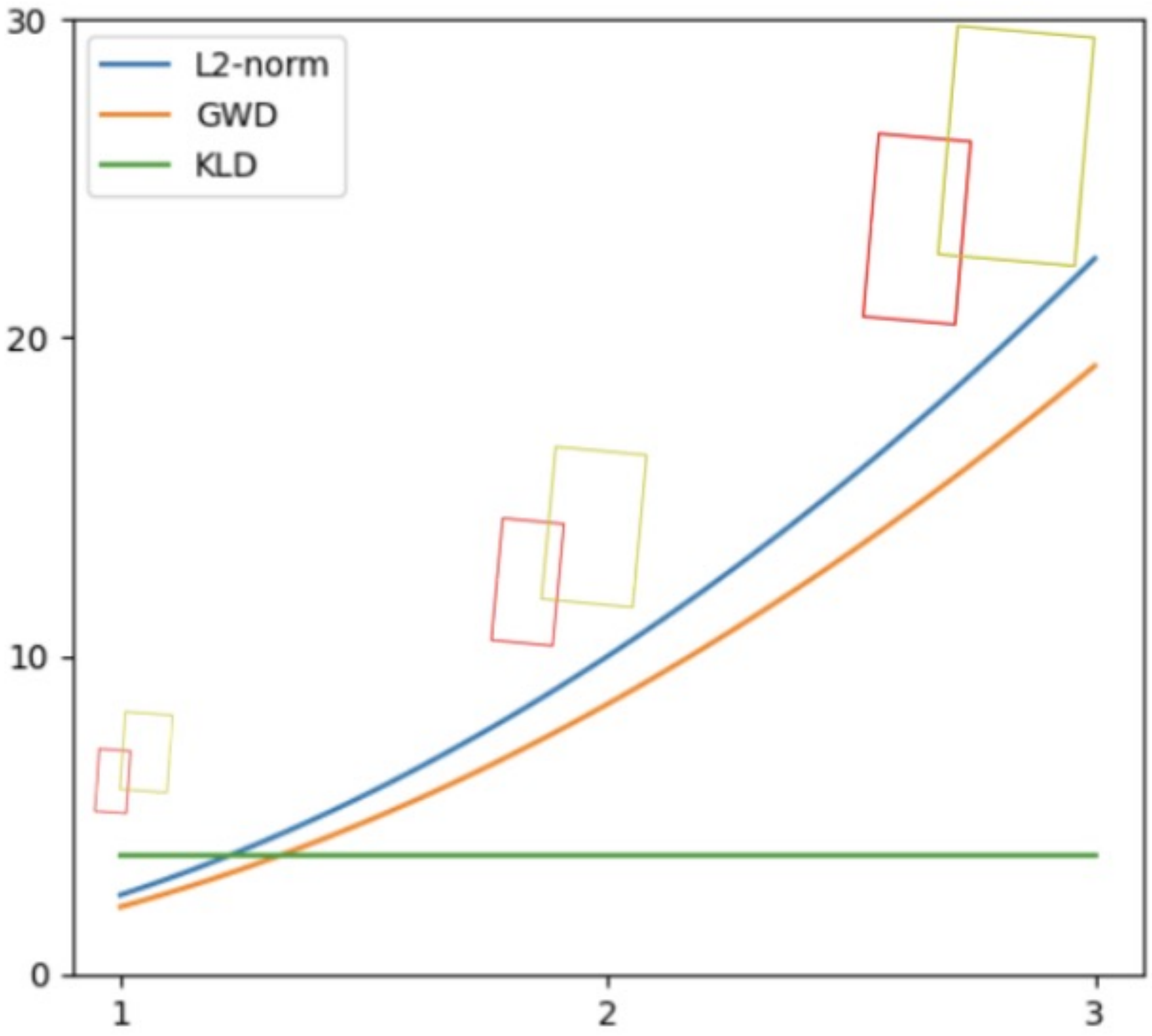

NEURAL INFORMATION PROCESSING SYSTEMS

Some Important Experiments

- After conducting high-precision detection experiments on 3 data sets and 2 detectors, we found that KLD almost beats the other two loss functions.

Table 3: High-precision detection experiment under different regression loss. 'R', 'F' and 'G' indicate random rotation, flipping, and graying, respectively.

Method	Dataset	Data Aug.	Reg. Loss	$Hmean_{50}/AP_{50}$	$Hmean_{60}/AP_{60}$	$Hmean_{75}/AP_{75}$	$Hmean_{85}/AP_{85}$	$Hmean_{50:95}/AP_{50:95}$
RetinaNet	HRSC2016	R+F+G	Smooth L1	84.28	74.74	48.42	12.56	47.76
			GWD	85.56 (+1.28)	84.04 (+9.30)	60.31 (+11.89)	17.14 (+4.58)	52.89 (+5.13)
			KLD	**87.45** (+3.17)	**86.72** (+11.98)	**72.39** (+23.97)	**27.68** (+15.12)	**57.80** (+10.04)
R^3Det			Smooth L1	88.52	79.01	43.42	4.58	46.18
			GWD	89.43 (+0.91)	88.89 (+9.88)	65.88 (+22.46)	15.02 (+10.44)	56.07 (+9.89)
			KLD	**89.97** (+1.45)	**89.73** (+10.72)	**77.38** (+33.96)	**25.12** (+20.54)	**61.40** (+15.22)
RetinaNet	MSRA-TD500	R+F+G	Smooth L1	70.98	62.42	36.73	12.56	37.89
			GWD	76.76 (+5.78)	68.58 (+6.16)	44.21 (+7.48)	17.75 (+5.19)	43.62 (+5.73)
			KLD	**76.96** (+5.98)	**70.08** (+7.66)	**46.95** (+10.22)	**19.59** (+7.03)	**45.24** (+7.35)
	ICDAR2015	F	Smooth L1	69.78	64.15	36.97	8.71	37.73
			GWD	74.29 (+4.51)	68.34 (+4.19)	43.39 (+6.42)	10.50 (+1.79)	41.68 (+3.95)
			KLD	**75.32** (+5.54)	**69.94** (+5.79)	**44.46** (+7.49)	**10.70** (+1.99)	**42.68** (+4.95)
		R+F	Smooth L1	74.83	69.46	42.02	11.59	41.98
			GWD	76.15 (+1.32)	71.26 (+1.80)	**45.59** (+3.57)	**11.65** (+0.06)	43.58 (+1.60)
			KLD	**77.92** (+3.09)	**72.77** (+3.31)	43.27 (+1.25)	11.09 (-0.50)	**43.65** (+1.67)
R^3Det		F	Smooth L1	74.28	68.12	35.73	8.01	39.10
			GWD	75.59 (+1.31)	68.36 (+0.24)	40.24 (+4.51)	9.15 (+1.14)	40.80 (+1.70)
			KLD	**77.72** (+2.43)	**71.99** (+3.87)	**43.95** (+8.22)	**10.43** (+2.42)	**43.29** (+4.19)
		R+F	Smooth L1	75.53	69.69	37.69	9.03	40.56
			GWD	77.09 (+1.56)	71.52 (+1.83)	41.08 (+3.39)	10.10 (+1.07)	42.17 (+1.61)
			KLD	**79.63** (+4.63)	**73.30** (+3.61)	**43.51** (+5.82)	**10.61** (+1.58)	**43.61** (+3.05)

Some Important Experiments

- We conducted verification experiments on some more challenging datasets, such as DOTA-v1.5 and DOTA-v2.0 (including many tiny objects less than 10 pixels). KLD still performs best.

Table 5: Accuracy comparison between different rotation detectors on DOTA dataset. † and ‡ represent the large aspect ratio object and the square-like object, respectively. The bold **red** and **blue** fonts indicate the top two performances respectively. D_{oc} and D_{le} represent OpenCV Definition ($\theta \in [-90°, 0°)$) and Long Edge Definition ($\theta \in [-90°, 90°)$) of RBox.

Baseline	Method	Box Def.	v1.0 tranval/test									v1.0 train/val			v1.5	v2.0
			BR†	SV†	LV†	SH†	HA†	ST‡	RA‡	7-AP$_{50}$	AP$_{50}$	AP$_{50}$	AP$_{75}$	AP$_{50:95}$	AP$_{50}$	AP$_{50}$
RetinaNet	-	D_{oc}	42.17	65.93	51.11	72.61	53.24	78.38	62.00	60.78	65.73	64.70	32.31	34.50	58.87	44.16
	-	D_{le}	38.31	60.48	49.77	68.29	51.28	78.60	60.02	58.11	64.17	62.21	26.06	31.49	56.10	43.06
	IoU-Smooth L1 [3]	D_{oc}	44.32	63.03	51.25	72.78	56.21	77.98	63.22	61.26	66.99	64.61	34.17	36.23	59.16	46.31
	Modulated Loss [43]	D_{oc}	42.92	67.92	52.91	72.67	53.64	**80.22**	58.21	61.21	66.05	63.50	33.32	34.61	57.75	45.17
	Modulated Loss [43]	Quad.	43.21	70.78	54.70	72.68	**60.99**	79.72	62.08	63.45	67.20	65.15	40.59	**39.12**	**61.42**	**46.71**
	RIL [32]	Quad.	40.81	67.63	55.45	72.42	55.49	78.09	64.75	62.09	66.06	64.07	**40.98**	39.05	58.91	45.35
	CSL [4]	D_{le}	42.25	68.28	54.51	72.85	53.10	75.59	58.99	60.80	67.38	64.40	32.58	35.04	58.55	43.34
	DCL (BCL) [44]	D_{le}	41.40	65.82	56.27	73.80	54.30	79.02	60.25	61.55	67.39	**65.93**	35.66	36.71	59.38	45.46
	GWD [5]	D_{oc}	**44.07**	**71.92**	**62.56**	**77.94**	60.25	79.64	**63.52**	**65.70**	**68.93**	65.44	38.68	38.71	60.03	46.65
	KLD	D_{oc}	**44.00**	**74.45**	**72.48**	**84.30**	**65.54**	**80.03**	**65.05**	**69.41**	**71.28**	**68.14**	**44.48**	**42.15**	**62.50**	**47.69**
R^{3}Det [26]	-	D_{oc}	44.15	75.09	72.88	86.04	56.49	82.53	61.01	68.31	70.66	67.18	38.41	38.46	62.91	48.43
	DCL (BCL) [44]	D_{le}	**46.84**	74.87	74.96	85.70	57.72	**84.06**	**63.77**	69.70	71.21	67.45	35.44	37.54	61.98	48.71
	GWD [5]	D_{oc}	46.73	**75.84**	**78.00**	**86.71**	**62.69**	**83.09**	61.12	**70.60**	**71.56**	**69.28**	**43.35**	**41.56**	**63.22**	**49.25**
	KLD	D_{oc}	**48.34**	**75.09**	**78.88**	**86.52**	**65.48**	82.08	**61.51**	**71.13**	**71.73**	**68.87**	**44.48**	**42.11**	**65.18**	**50.90**

Some Important Experiments

- In the horizontal detection task (COCO dataset), KLD also maintains a similar level with commonly used loss functions, such as GIoU.

Table 6: Performance evaluation of KLD on classic horizontal detection.

Detector	Reg. Loss	AP	AP_{50}	AP_{75}	AP_s	AP_m	AP_l	Detector	Reg. Loss	AP	AP_{50}	AP_{75}	AP_s	AP_m	AP_l
RetinaNet	Smooth L1	37.2	56.6	39.7	21.4	41.1	48.0	Faster RCNN	Smooth L1	37.9	58.8	41.0	22.4	41.4	49.1
	GIoU	37.4	56.7	39.7	22.2	41.7	48.1		GIoU	**38.3**	58.7	41.5	22.5	41.7	49.7
	KLD	**38.0**	56.4	40.6	23.3	43.2	49.3		KLD	38.2	58.7	41.7	22.6	41.8	49.3

- We conducted experiments on different variants of KLD on two datasets, and found that the final performance was similar, eliminating the interference of asymmetry on the results.

Table 2: Ablation of different KLD-based regression loss form. The based detector is RetinaNet.

Dataset	$\mathbf{D}_{kl}(\mathcal{N}_p\|\|\mathcal{N}_t)$	$\mathbf{D}_{kl}(\mathcal{N}_t\|\|\mathcal{N}_p)$	$\mathbf{D}_{kl\_min}(\mathcal{N}_p\|\|\mathcal{N}_t)$	$\mathbf{D}_{kl\_max}(\mathcal{N}_p\|\|\mathcal{N}_t)$	$\mathbf{D}_{js}(\mathcal{N}_p\|\|\mathcal{N}_t)$	$\mathbf{D}_{jeffreys}(\mathcal{N}_p\|\|\mathcal{N}_t)$
DOTA-v1.0	70.17	70.64	**70.71**	70.55	69.67	70.56
HRSC2016	82.83	83.82	83.60	82.70	**84.06**	83.66

Some Important Experiments

➢ Finally, in the SOTA experiment of DOTA-v1.0, we also achieved the highest performance in the current published papers.

Table 7: AP on different objects on DOTA-v1.0. Here R-101 denotes ResNet-101 (likewise for R-50, R-152), and RX-101 and H-104 represent ResNeXt101 [46] and Hourglass-104 [47], respectively. MS indicates that multi-scale training/testing is used. **Red** and **blue** indicate the top two performances.

	Method	Backbone	MS	PL	BD	BR	GTF	SV	LV	SH	TC	BC	ST	SBF	RA	HA	SP	HC	AP_{50}
Two-stage	ICN [29]	R-101	✓	81.40	74.30	47.70	70.30	64.90	67.80	70.00	90.80	79.10	78.20	53.60	62.90	67.00	64.20	50.20	68.20
	RoI-Trans. [11]	R-101	✓	88.64	78.52	43.44	75.92	68.81	73.68	83.59	90.74	77.27	81.46	58.39	53.54	62.83	58.93	47.67	69.56
	SCRDet [3]	R-101	✓	89.98	80.65	52.09	68.36	68.36	60.32	72.41	90.85	87.94	86.86	65.02	66.68	66.25	68.24	65.21	72.61
	Gliding Vertex [48]	R-101		89.64	85.00	52.26	77.34	73.01	73.14	86.82	90.74	79.02	86.81	59.55	70.91	72.94	70.86	57.32	75.02
	Mask OBB [49]	RX-101	✓	89.56	85.95	54.21	72.90	76.52	74.16	85.63	89.85	83.81	86.48	54.89	69.64	73.94	69.06	63.32	75.33
	CenterMap OBB [50]	R-101	✓	89.83	84.41	54.60	70.25	77.66	78.32	87.19	90.66	84.89	85.27	56.46	69.23	74.13	71.56	66.06	76.03
	FPN-CSL [4]	R-152	✓	90.25	85.53	54.64	75.31	70.44	73.51	77.62	90.84	86.15	86.69	69.60	68.04	73.83	71.10	68.93	76.17
	RSDet-II [43]	R-152	✓	89.93	84.45	53.77	74.35	71.52	78.31	78.12	91.14	87.35	86.93	65.64	65.17	75.35	79.74	63.31	76.34
	SCRDet++ [51]	R-101	✓	90.05	84.39	55.44	73.99	77.54	71.11	86.05	90.67	87.32	87.08	69.62	68.90	73.74	71.29	65.08	76.81
	ReDet [52]	ReR-50	✓	88.81	82.48	60.83	80.82	78.34	86.06	88.31	90.87	88.77	87.03	68.65	66.90	79.26	79.71	74.67	80.10
Single-stage	PIoU [30]	DLA-34 [53]		80.90	69.70	24.10	60.20	38.30	64.40	64.80	90.90	77.20	70.40	46.50	37.10	57.10	61.9	64.00	60.50
	O^2-DNet [54]	H-104	✓	89.31	82.14	47.33	61.21	71.32	74.03	78.62	90.76	82.23	81.36	60.93	60.17	58.21	66.98	61.03	71.04
	DAL [14]	R-101	✓	88.61	79.69	46.27	70.37	65.89	76.10	78.53	90.84	79.98	78.41	58.71	62.02	69.23	71.32	60.65	71.78
	P-RSDet [55]	R-101	✓	88.58	77.83	50.44	69.29	71.10	75.79	78.66	90.88	80.10	81.71	57.92	63.03	66.30	69.77	63.13	72.30
	BBAVectors [56]	R-101	✓	88.35	79.96	50.69	62.18	78.43	78.98	87.94	90.85	83.58	84.35	54.13	60.24	65.22	64.28	55.70	72.32
	DRN [13]	H-104	✓	89.71	82.34	47.22	64.10	76.22	74.43	85.84	90.57	86.18	84.89	57.65	61.93	69.30	69.63	58.48	73.23
	PolarDet [57]	R-101	✓	89.65	87.07	48.14	70.97	78.53	80.34	87.45	90.76	85.63	86.87	61.64	70.32	71.92	73.09	67.15	76.64
	RDD [58]	R-101	✓	89.15	83.92	52.51	73.06	77.81	79.00	87.08	90.62	86.72	87.15	63.96	70.29	76.98	75.79	72.15	77.75
	GWD [5]	R-152	✓	89.06	84.32	55.33	77.53	76.95	70.28	83.95	89.75	84.51	86.06	73.47	67.77	72.60	75.76	74.17	77.43
	KLD	R-50		88.91	83.71	50.10	68.75	78.20	76.05	84.58	89.41	86.15	85.28	63.15	60.90	75.06	71.51	67.45	75.28
		R-50	✓	88.91	85.23	53.64	81.23	78.20	76.99	84.58	89.50	86.84	86.38	71.69	68.06	75.95	72.23	75.42	78.32
Refine-stage	CFC-Net [31]	R-101	✓	89.08	80.41	52.41	70.02	76.28	78.11	87.21	90.89	84.47	85.64	60.51	61.52	67.82	68.02	50.09	73.50
	R^3Det [26]	R-152	✓	89.80	83.77	48.11	66.77	78.76	83.27	87.84	90.82	85.38	85.51	65.67	62.68	67.53	78.56	72.62	76.47
	DAL [14]	R-50	✓	89.69	83.11	55.03	71.00	78.30	81.90	88.46	90.89	84.97	87.46	64.41	65.65	76.86	72.09	64.35	76.95
	DCL [44]	R-152	✓	89.26	83.60	53.54	72.76	79.04	82.56	87.31	90.67	86.59	86.98	67.49	66.88	73.29	70.56	69.99	77.37
	RIDet [32]	R-50	✓	89.31	80.77	54.07	76.38	79.81	81.99	89.13	90.72	83.58	87.22	64.42	67.56	78.08	79.17	62.07	77.62
	S^2A-Net [12]	R-101	✓	89.28	84.11	56.95	79.21	80.18	82.93	89.21	90.86	84.66	87.61	71.66	68.23	78.58	78.20	65.55	79.15
	R^3Det-GWD [5]	R-152	✓	89.66	84.99	59.26	82.19	78.97	84.83	87.70	90.21	86.54	86.85	73.04	67.56	76.92	79.22	74.92	80.19
	R^3Det-KLD	R-50		88.90	84.17	55.80	69.35	78.72	84.08	87.00	89.75	84.32	85.73	64.74	61.80	76.62	78.49	70.89	77.36
		R-50	✓	89.90	84.91	59.21	78.74	78.82	83.95	87.41	89.89	86.63	86.69	70.47	70.87	76.96	79.40	78.62	80.17
		R-152	✓	89.92	85.13	59.19	81.33	78.82	84.38	87.50	89.80	87.33	87.00	72.57	71.35	77.12	79.34	78.68	80.63

NEURAL INFORMATION PROCESSING SYSTEMS

- Paper: https://arxiv.org/abs/2106.01883
- Code: https://github.com/yangxue0827/RotationDetection
- Contact:

  - Xue Yang: yangxue-2019-sjtu@sjtu.edu.cn
  - Junchi Yan: yanjunchi@sjtu.edu.cn

- Homepage of our Lab:
  - http://thinklab.sjtu.edu.cn/